Automated Operational Forecasting of Monsoon Low Pressure Systems

D. L. Suhas,[a] S. Vishnu,[b] Salil Goyal,[c] Sahadat Sarkar,[d] Parthasarathi Mukhopadhyay,[d,e] Paul A. Ullrich,[f,g] and William R. Boos[a,h]

ABSTRACT: Monsoon low pressure systems (LPSs) are the dominant rain-bearing weather system of South Asia, often producing extreme precipitation and hydrological disasters in a region inhabited by nearly two billion people. Despite the importance of these storms, no operational system has automatically identified and tracked LPS in real time in numerical weather prediction model output; many commonly used vortex-tracking algorithms are ill suited for monsoon LPS because of the weak winds and cold cores of these systems. Here, we describe a new system that uses optimized algorithms to identify monsoon LPS in short- to medium-range forecasts from the U.S. Global Ensemble Forecast System (GEFS) and a version of the deterministic Global Forecast System (GFS) adapted and used operationally by the Indian Institute of Tropical Meteorology (IITM). We also assess the historical performance of these models in forecasting South Asian monsoon LPS, comparing this with the performance of the Integrated Forecasting System of the ECMWF. We assess the accuracy of model predictions of LPS genesis, position, intensity, and precipitation rates for forecast lead times of 1–5 days, yielding quantitative information on model biases to guide operational forecasters and disaster managers. The system we introduce here could be extended to other low-latitude regions affected by dynamically weak, heavily precipitating atmospheric vortices that are often not included in tropical cyclone inventories.

SIGNIFICANCE STATEMENT: South Asia frequently experiences intense rainfall and hydrological disasters produced by atmospheric vortices known as monsoon low pressure systems (LPSs). In this work, we introduce the first automated system that uses numerical weather prediction model output with a tracking algorithm optimized for the characteristically weak winds of monsoon LPS, producing operational forecasts of these storms. This system provides forecasts of LPS positions, intensities, and rain rates with accuracies that we quantify here, offering valuable information for forecasters and disaster managers that serve the nearly two billion people living in South Asia.

AFFILIATIONS: [a] Department of Earth and Planetary Science, University of California, Berkeley, Berkeley, California; [b] School of Earth Environmental and Sustainability Sciences, Indian Institute of Science Education and Research, Thiruvananthapuram, India; [c] Department of Mathematics, University of California, Berkeley, Berkeley, California; [d] Indian Institute of Tropical Meteorology, Ministry of Earth Sciences, Pune, India; [e] Department of Earth and Environmental Sciences, Indian Institute of Science Education and Research, Berhampur, Odisha, India; [f] Department of Land, Air and Water Resources, University of California, Davis, Davis, California; [g] Computational Research Division, Lawrence Berkeley National Laboratory, Berkeley, California; [h] Climate and Ecosystem Sciences Division, Lawrence Berkeley National Laboratory, Berkeley, California

1. Introduction

On the banks of the Mandakini River in the western Himalayas lies Kedarnath, a small Indian town visited by hundreds of thousands of tourists each summer (Mahanti 2022; Sati 2020). Over 4 days in June 2013, nearly a meter of rain fell on Kedarnath and thousands of surrounding villages (Dobhal et al. 2013; Houze et al. 2017), triggering flash floods and landslides that caused over 6000 deaths and affected half a million people (Guha-Sapir et al. 2015; Sati and Gahalaut 2013). Such hydrological extremes occur every few years in South Asia (Nikumbh et al. 2020), with other examples being the 0.94 m of rain in Mumbai on 26 July 2005 (Kumar et al. 2008), the 2010 Pakistan floods (Houze et al. 2011), the 2015 Chennai floods (Chakraborty 2016), and the 2018 Kerala disaster (Hunt and Menon 2020; Mukhopadhyay et al. 2021). Common to all of these examples is the presence of a monsoon low pressure system (LPS), a transient atmospheric vortex that produces intense precipitation (Sikka 1977) and is associated with more than half of South Asia's hydrometeorological disasters (Suhas et al. 2023).

Monsoon LPSs are cyclonic vortices with typical outer diameters exceeding 2000 km. These transient storms form within the larger-scale summer monsoon circulations of South Asia (Mooley and Shukla 1987) and Australia (Davidson and Holland 1987) and have some dynamical similarity with the vortices and easterly waves that form in the east Pacific (Hurley and Boos 2015; Fig. 1a places South Asian monsoon LPS in the global context of low-latitude cyclonic vortices). Early work hypothesized that the strong vertical or horizontal wind shears of continental-scale monsoon circulations create LPS through one of several possible hydrodynamic instabilities (Rao and Rajamani 1970; Krishnamurti et al. 1976). More recent analyses have shown that LPS amplification primarily results from barotropic instability of the lower-tropospheric monsoon westerly jet, with advection of water vapor by the vortex winds also playing an important role (Diaz and Boos 2019a, 2021; Adames and Ming 2018; Suhas and Boos 2023; Luo et al. 2023). This formation mechanism can explain the observed spatial concentration of LPS over the northern Bay of Bengal during boreal summer (Figs. 1a,b), where strong climatological-mean horizontal wind shear and high moisture content coincide with the global maxima of LPS genesis and track densities (Sikka 2006; Ditchek et al. 2016). The barotropic instability and moisture-advection mechanisms described above also explain the typical westward propagation of LPS over continental India during the 5–10-day lifetime of these storms (see sample tracks in Fig. 1b).

Monsoon LPSs have dynamics, spatial structures, and intensities that render them distinct from the canonical population of tropical cyclones, which in turn are rarely observed in
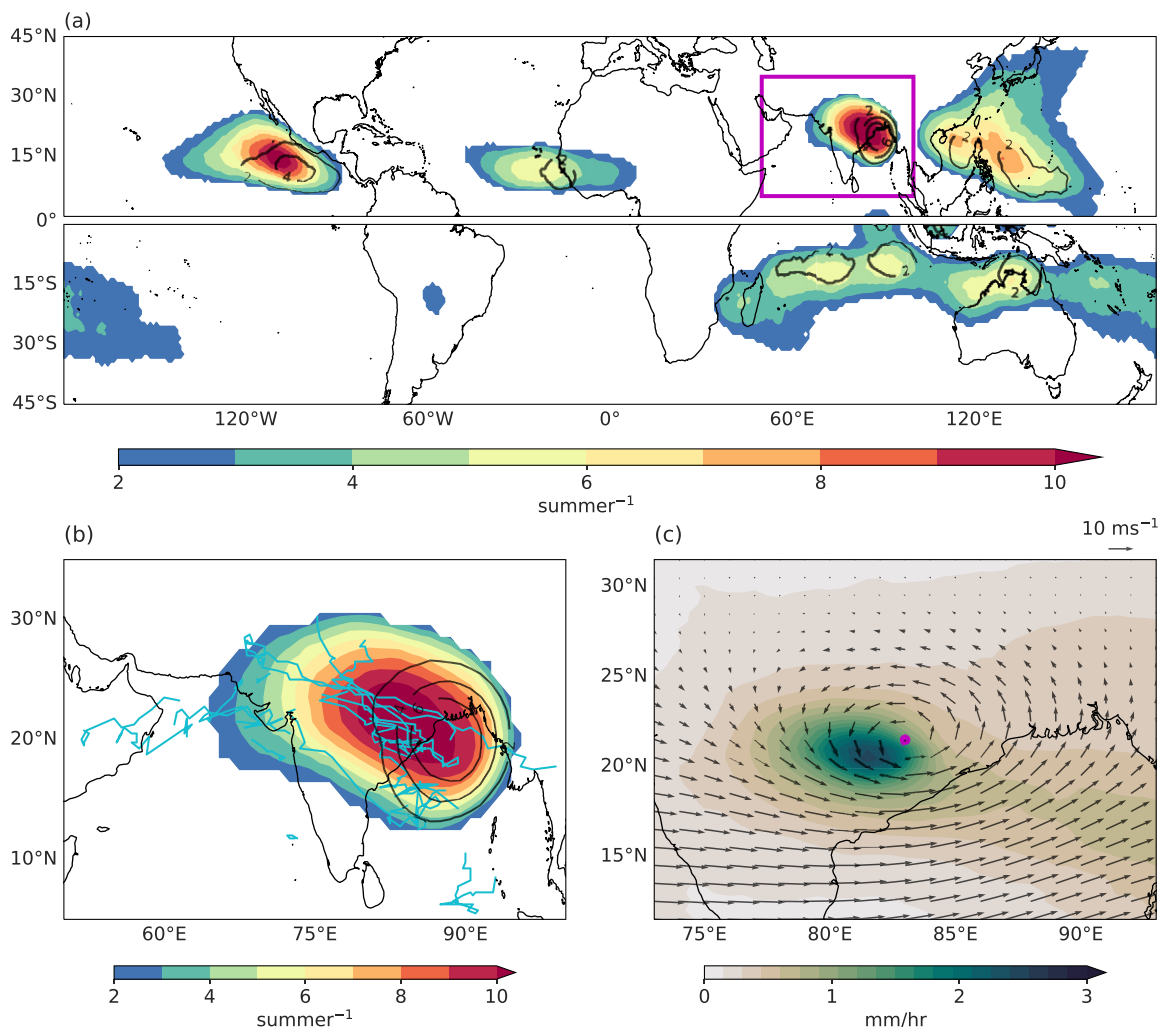
FIG. 1. (a) Climatology of LPS genesis density (black contours) and track density (shading) from ERA5 (1979–2022) in local summer (June–September for the Northern Hemisphere; December–March for the Southern Hemisphere), with densities being the mean number per season of genesis points and tracks within 5° of each geographic location. The magenta box shows the domain considered in this study, which contains mainly monsoon LPS. (b) LPS tracks for the year 2022 (cyan lines) overlaid on the same quantities as in (a), for the South Asian region. (c) Composite-mean vortex-centered precipitation (shading; mm h⁻¹; IMERG) for South Asian LPS in June–September 2000–22, with the storm center (magenta dot) depicted at the median position of all LPSs in geographic coordinates. Storm-centered precipitation is computed within a 20° × 20° box centered on the LPS track. Vectors show vortex-centered composite-mean ERA5 850-hPa winds. The algorithm used to obtain the tracks shown here is described in section 2, optimizing monsoon low pressure system tracking.

South Asia during summer because of the strong vertical shear of the large-scale monsoon (Gray 1968). The surface winds of monsoon LPSs are so weak, typically 5–10 m s⁻¹, that fewer than 20% of South Asian monsoon LPSs can be found in best track datasets of tropical cyclones (Haertel and Boos 2017); the population of cyclonic disturbances in other regions, such as the Atlantic and Pacific (Fig. 1a), may be more heavily dominated by traditional tropical cyclones. The dynamical weakness of monsoon LPS makes some vortex-tracking algorithms—which are tuned to automatically identify tropical cyclones in atmospheric data—ill suited for these storms (see next section). Monsoon LPSs are also distinct from canonical tropical cyclones in that they have a lower-tropospheric cold core, which can be explained by their formation through barotropic instability (Diaz and Boos 2019a), and can transit land surfaces without appreciable loss of intensity (Sikka 1977). Their precipitation is typically concentrated southwest of the vortex center (Fig. 1c) due to dynamical lifting produced by the interaction of the cyclonic vortex with the background vertical shear

(Rao and Rajamani 1970; Sanders 1984), an effect similar to but more pronounced than that seen in tropical cyclones in vertical shear (e.g., Jones 1995).

Accurately forecasting the location and intensity of monsoon LPS is vital for providing early disaster warnings to the nearly two billion people that inhabit the South Asian monsoon domain. While tropical cyclones are routinely identified by operational, automated algorithms in forecasts made by numerical weather prediction (NWP) systems (Cangialosi 2021; Sampson and Schrader 2000; Yu et al. 2013), no analogous effort has been made for monsoon LPS. This is true despite the large human population affected by these storms, perhaps in part because of the difficulty of tracking such dynamically weak systems. Recent research has confirmed the potential utility of short- and medium-term NWP forecasts of LPS tracks and precipitation for providing early warning of hydrological disasters in South Asia (Suhas et al. 2023). Thus, there is a compelling need for an operational, real-time forecasting system for monsoon LPS. Here, we describe such a system, developed through an international partnership, that uses short- to medium-range forecasts from NWP models run operationally in India and the United States.

For operational forecasts of monsoon LPS to be of practical use, the accuracy of those forecasts must be known. We are aware of only two studies that analyzed the fidelity of operational NWP models in forecasting monsoon LPS. Sarkar et al. (2021) studied a version of NCEP's GFS model that was modified by the Indian Institute of Tropical Meteorology (GFS-IITM) and is used operationally by the India Meteorological Department. The GFS-IITM model performed well in simulating the dynamics involved in the transition of weaker LPS (called monsoon lows) to stronger LPS (called monsoon depressions) but performed more poorly in forecasting the dynamics of monsoon lows that did not intensify to depression strength. However, Sarkar et al. (2021) did not assess the model's accuracy in predicting LPS position, intensity, or rain rate. Deoras et al. (2021) assessed South Asian monsoon LPS forecasts in the Subseasonal to Seasonal Prediction project (S2S), finding that S2S models underestimated the frequency of LPS and were underdispersive in their forecasts of LPS position and intensity relative to ERA-Interim and MERRA-2 reanalyses. While Deoras et al. (2021) compared the climatological-mean spatial distributions of genesis density in the S2S models with reanalyses, they did not assess the model ability to correctly forecast actual genesis events near the location and time they were observed. Deoras et al. (2021) also did not compare storm-centered rain rates with observations (although they did assess how seasonal mean precipitation errors in models covaried with LPS occurrence) and did not examine the accuracy of the NWP models used operationally by Indian institutions.

The operational system introduced here identifies monsoon LPS in forecasts from the GFS-IITM model (mentioned above) and the NCEP Global Ensemble Forecast System (GEFS). To provide practical guidance for forecast end users, we evaluate the historical performance of these models, as well as that of the ECMWF Integrated Forecasting System (IFS), by comparing them with LPS tracks from the ERA5 reanalysis. This assessment focuses on the models' ability to predict the genesis, location, intensity, and precipitation rates of South Asian LPS. The results presented here build on previous optimization and validation of an LPS tracking algorithm (Vishnu et al. 2020) and assessment of the accuracy of GEFS-based probabilistic ensemble forecasts of LPS genesis (Suhas and Boos 2024).

2. Optimizing monsoon low pressure system tracking

Numerous algorithms are routinely used to identify a broad range of atmospheric phenomena in gridded data (Leung et al. 2022). Algorithms that track tropical cyclones seem most relevant for monsoon LPS, which might be viewed as weak tropical depressions (the weakest tropical cyclone category on the Saffir–Simpson scale) embedded in strongly sheared monsoon flow.

However, algorithms optimized for warm-core tropical cyclones may not work well for monsoon LPS, which have low-level cold cores and comparatively weak surface winds of $\sim 5–10\,\mathrm{m\,s^{-1}}$. When one tropical cyclone-tracking algorithm was used to detect South Asian monsoon LPS in ERA-Interim data, it found about half as many storms as in a human-analyzed track dataset (Dong et al. 2020; Sikka 2006).

The need for a tracking algorithm optimized for monsoon LPS motivated a systematic assessment by Vishnu et al. (2020) of candidate input variables and algorithmic details. Those authors then developed a scheme, which is deployed operationally here, that identifies LPS using TempestExtremes (Ullrich et al. 2021), software that uses parallel processing to rapidly find closed contours of a specified magnitude in data of arbitrarily high resolution. Vishnu et al. (2020) found that South Asian monsoon LPSs were best detected using the streamfunction of the 850-hPa horizontal wind, a smoother and less resolution-dependent variable than vorticity (i.e., the Laplacian of the streamfunction), which is often used to track vortices (e.g., Hurley and Boos 2015; Hunt and Fletcher 2019). Monsoon LPSs can be difficult to distinguish from the noisy background vorticity field but are clearly evident as streamfunction minima. Figure 2 uses ERA5 data to illustrate this for the storm in the below case study, showing that streamfunction-based tracking yields a longer track that better matches the India Meteorological Department's subjective analysis. In contrast, vorticity-based tracking abruptly shifts the storm center

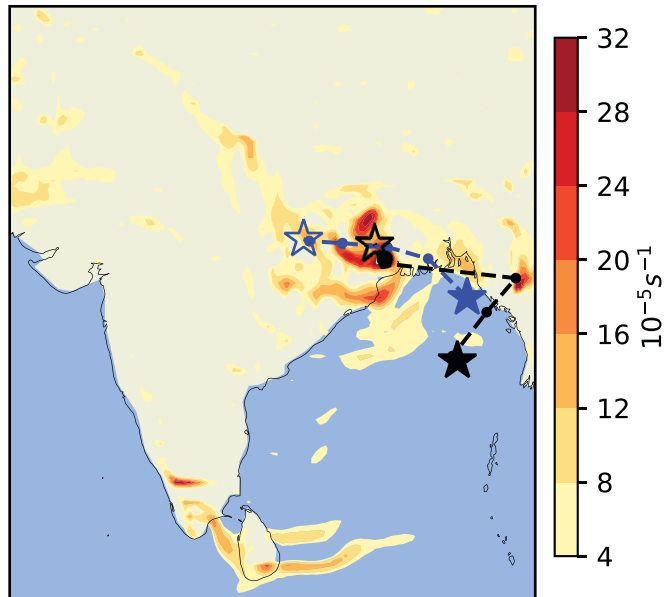## (a) Streamfunction
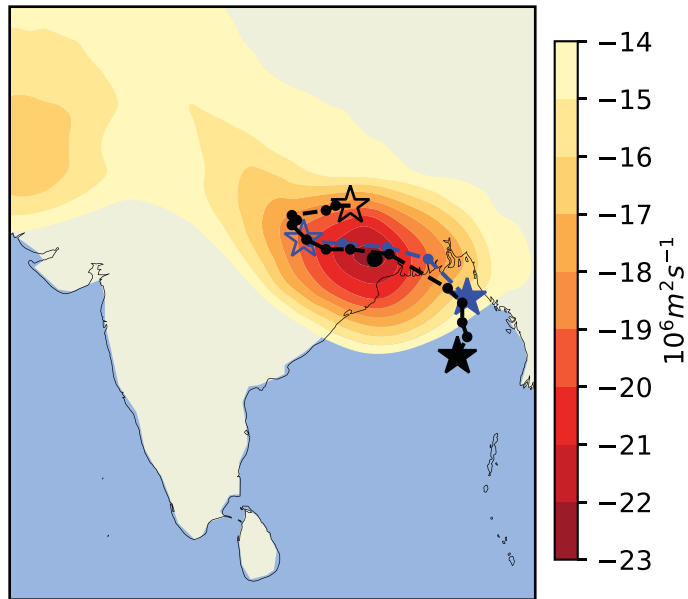
(b) Vorticity

FIG. 2. Illustration of LPS tracking performed using ERA5 850-hPa (a) streamfunction (m² s⁻¹) and (b) vorticity (s⁻¹), with these variables shown by shading at 0600 UTC 2 Aug 2023, when the storm in this case study achieved its minimum SLP (i.e., maximum intensity). Black dashed lines show tracks identified by our algorithm using the respective variable, with filled stars representing the starting location at 0600 UTC 30 Jul 2023, open stars marking the end of the track, large circles indicating the storm center location when streamfunction and vorticity are shown, and 12-h track positions marked by small circles (in contrast, Fig. 3 shows tracks based on 6-h data). Blue lines show the subjectively analyzed track from the India Meteorological Department, with symbols having the same meaning as the black lines.

to a peripheral vorticity maximum east of the Bay of Bengal shortly after genesis and then terminates the track prior to the last few days of the storm's inland, rain-producing lifetime.

Using streamfunction as a tracking variable also does not involve assumptions of geostrophic balance, which are implicit when using geopotential or sea level pressure (SLP) to infer a vortex's circulation. Unlike SLP, the 850-hPa streamfunction furthermore directly represents the strongest winds in monsoon LPS, which typically occur at 2–4-km altitude. Using 40 years of data from five reanalyses, this algorithm produced LPS tracks that agreed well with a hand-analyzed track dataset (Vishnu et al. 2020).

We define intensity metrics based on wind speed and storm central pressure, which are also used to classify LPS as monsoon lows (weaker LPS) or monsoon depressions (which here include all LPSs stronger than monsoon lows) following traditional criteria of the India Meteorological Department (Ajayamohan et al. 2010; Hurley and Boos 2015). A depression must achieve peak surface winds greater than 8.5 m s^{-1} within 3° of the storm center and a central SLP at least 4 hPa below the SLP on the storm's periphery (for details, see Vishnu et al. 2020). We call this SLP anomaly the "pressure drop," measuring it as the magnitude of the largest closed contour of SLP anomaly that can be drawn around the SLP minimum within a 10° radius of that minimum, with the SLP minimum located within 3° of the streamfunction minimum (Ullrich et al. 2021; Vishnu et al. 2020). The original algorithm also required LPS to achieve a minimum 850-hPa relative humidity of 85% along their track to distinguish these systems from desert heat lows. As the GEFS and GFS-IITM models systematically underestimate lower-tropospheric relative humidity over India (Mukhopadhyay et al. 2019), here we use a relative humidity threshold of 80% in those models.

3. Implementing the operational system

a. Data sources and model details. The system uses short- to medium-term forecasts from the 31-member GEFS v12 developed by the NCEP (Zhou et al. 2022), as well as the deterministic GFS-IITM model. The GEFS model is initialized four times daily and uses a cubed-sphere grid of ~25-km horizontal grid spacing with 64 sigma–pressure hybrid levels. The control run is initialized with the hybrid GFS analysis, whereas ensemble members are initialized with the analysis perturbed by the 6-h EnKF forecast ensemble (Zhou et al. 2022). The GFS-IITM model is a version of NCEP's GFS model, run operationally at the IITM since June 2016. It employs a spectral T1534 grid (nominal 12.5 km grid spacing) with 64 hybrid vertical levels and is initialized twice daily at 0000 and 1200 UTC (Mukhopadhyay et al. 2019). India's National Centre for Medium Range Weather Forecasting (NCMRWF) generates initial conditions using the Global Data Assimilation System (GDAS) cycle, incorporating denser observations in the Indian region (Prasad et al. 2016). All of these descriptions refer to the operational model versions at the time of writing, which may differ from those used to produce archived forecasts or those operational after publication.

We compare forecasts from the above two models with those from the ECMWF IFS. However, we have not implemented operational tracking of monsoon LPS in ECMWF forecasts because those are not publicly available in real time. The ECMWF model is also spectral in nature, and its latest version uses the O1280 octahedral grid (nominally 9 km in the horizontal) with 137 vertical levels. The model is initialized twice daily at 0000 and 1200 UTC using ECMWF 4D-Var data assimilation.

For consistency in our analyses, we use model outputs at a horizontal grid spacing of 0.5° and focus solely on forecasts initialized at 0000 UTC. We obtained the GEFS and ECMWF forecasts from the TIGGE archive (Park et al. 2008; Bougeault et al. 2010; Swinbank et al. 2016), which provides GEFS forecasts for lead times up to 16 days and ECMWF forecasts for lead times up to 15 days. The GEFS output was stored in the TIGGE archive at 0.5° grid spacing, while ECMWF output was linearly interpolated to that grid spacing by the archive's

retrieval system. GFS-IITM forecasts were available at a 0.125° grid spacing for a lead time of 10 days; bilinear interpolation was used to increase the grid spacing to 0.5° for all variables except precipitation, for which conservative regridding was used. For the best comparison with the GFS-IITM deterministic model, we only assess the accuracy of control runs from the GEFS and ECMWF models, leaving an examination of ensemble genesis forecasts for separate work (Suhas and Boos 2024). We assess model accuracy during the June–September monsoon season, from 2016 (the year of operational deployment of the GFS-IITM model) to 2022. Due to limitations in transferring large volumes of data from India to the U.S. site of analysis, we limited our analysis of the GFS-IITM model to forecasts initialized 0–120 h before the genesis of observed LPS. Since forecasts for some initialization dates are thus omitted for the GFS-IITM model, we do not calculate a false alarm metric for that model. For the control runs of the GEFS and ECMWF models, an evaluation spanning all June–September days of the longer 2008–22 period is shown in Figs. S1 and S2 in the online supplemental material.

We evaluate the performance of forecasts from these models using LPS tracks from ERA5 (Hersbach et al. 2020) as the reference. Results using the MERRA-2 reanalysis (Gelaro et al. 2017) were similar (Figs. S3 and S4).[1] To assess the accuracy of model forecasts of LPS precipitation, we compare them with high-resolution (0.1° × 0.1° grid spacing), half-hourly precipitation estimates from the final run of the Integrated Multi-satellitE Retrievals for GPM (IMERG; Huffman et al. 2020).

---

[1] The atmospheric analysis most similar to the initial conditions of the GEFS model is expected to be the final operational global analysis (FNL) produced by NCEP's Global Data Assimilation System (GDAS), but LPS tracks have not been identified and validated in that analysis. In contrast, MERRA-2 and three other reanalyses were shown to have hit rates exceeding 80% when validated against a hand-analyzed LPS track dataset (Vishnu et al. 2020).

---

b. Track comparison methods. A model forecast track is considered to match a reanalysis track if the mean spatial separation between the first four points of the model track and the corresponding points in the reanalysis track that occur at the same time is less than 4° (Froude 2010; Hodges and Emerton 2015; Deoras et al. 2021). The genesis point is simply defined as the first point in time on each track, with tracks obtained by stitching together locations of streamfunction minima subject to spatiotemporal separation criteria (Vishnu et al. 2020). We require model forecast tracks to have genesis within 5 days of model initialization, thereby eliminating forecasts where genesis is predicted with lead times over 5 days. Subsequent analyses demonstrate that genesis-based metrics, such as the probability of detection and the false alarm ratio, have poor accuracy by 5 days of lead time. In cases where multiple tracks for a given model initialization time match the same reanalysis track, we select the model track with genesis closest in time to that of the reanalysis (Zhang et al. 2023). Additionally, if a model's track matches multiple reanalysis tracks, we choose the reanalysis track with the minimum mean spatial separation from the model forecast.

In our analysis of model accuracy, we use three time variables: forecast lead time, time prior to observed genesis, and observed time (i.e., real wall-clock time). Forecast lead time is the number of hours (or days) elapsed since forecast model initialization; this time variable is commonly used in analyses of forecasts and is the one we use in most metrics. However, when estimating the accuracy of genesis forecasts, we use the number of hours prior to the observed genesis time because our metrics are defined with respect to observed genesis events. Specifically, model genesis and observed genesis do not need to occur at the same time for forecasts to be deemed a match; e.g., a model initialized 2 days prior to the observed genesis of an LPS might forecast genesis 1 day before or 2 days after observed genesis and would be considered a match if the track met the distance criteria outlined above.

c. Operational workflow. The operational system provides forecasts based on both the GFS-IITM and GEFS models, with model integration and subsequent processing performed

in both India and the United States. Having access to forecasts from multiple models is usually desirable for human forecasters, motivating the use of both models. The GFS-IITM model is run operationally every day by the IITM. The automated workflow and tracking algorithm, developed at University of California (UC) Berkeley, are executed daily on an IITM computing cluster to transform pressure-level winds into the streamfunction, extract other variables (e.g., precipitation), and identify LPS tracks. Graphics are automatically generated, then transferred to a website hosted by UC Berkeley (https://worldmonsoons.org/LPStrackingSite/), and also posted on the IITM short-range prediction site (https://srf.tropmet.res.in/srf/hires_gefs/files/gfs_lps.php). A parallel workflow is run at UC Berkeley using the GEFS ensemble and then displayed on a separate page (http://worldmonsoons.org/LPStrackingSite/index_gefs.html) on the same UC Berkeley website. Graphics on that page differ from those on the GFS-IITM page in that they incorporate track probabilities and ensemble predictions for LPS intensities and rain rates.

4. Case study of a disastrous storm

We demonstrate the functionality of the operational system using a monsoon LPS from 2023. In ERA5 data, this LPS formed over the northern Bay of Bengal at 0600 UTC 30 July 2023 (gray dot in Fig. 3a). It then propagated northwestward and intensified enough to be included as the fourth storm in the IBTrACS archive of 2023 north Indian Ocean tropical cyclones; nevertheless, this LPS had a cold core in the lower troposphere for much of its lifetime and was not a named tropical cyclone. In IBTrACS, this feature lasted less than 24 h, spanning 1800 UTC 31 July 2023–1200 UTC 1 August 2023, while our algorithm identified a 7-day lifetime in ERA5 with a track stretching over 1000 km inland (gray line in Fig. 3a; see Fig. 2 for the India Meteorological Department track).

This storm produced heavy rainfall in eastern India, with 24-h accumulations exceeding 100 mm across large parts of the state of Odisha and reaching 390.6 mm at one station (Ministry of Home Affairs 2023a). This raised multiple rivers to a severe or extreme flood stage, affecting hundreds of thousands of people in nearly 2000 villages (Ministry of Home Affairs 2023b; Jha 2023; Press Trust of India 2023). A warning issued by the India Meteorological Department (discussed below) placed local authorities on high alert, and disaster response teams were deployed for search and rescue operations (Directorate General for Civil Protection and Humanitarian Aid Operations 2023). With at most 20 fatalities, the response to this storm provides an example of successful disaster risk reduction in Odisha, a region that experienced significant reforms in disaster preparedness and management following the loss of ~10 000 lives during a devastating tropical cyclone in October 1999 (Walch 2019).

The intensification and northwestward propagation of this LPS were first forecast by the India Meteorological Department at 0800 UTC 31 July 2023 (India Meteorological Department 2023), 1 day after the ERA5 starting point shown in Fig. 3a. The GEFS model successfully predicted key elements of this storm for an initialization time more than a full day earlier, at 0000 UTC 30 July 2023. The control run with that initialization time matched observed peak surface wind speeds for approximately 7 days of lead time and accurately predicted storm location over the first half of the track (Figs. 3a,d). When the control run track later deviated from the observed track, the peak track density of the perturbed ensemble members provided a better match. Similarly, although the control run did not predict the large reduction in LPS central pressure observed 2–4 days after forecast initialization, some ensemble members exhibited intensification that was nearly as strong as observed (Fig. 3c).

The GEFS control run predicted total rain accumulations of 50–200 mm over a region encompassing several Indian states and Bangladesh (Fig. 3b). The peak observed impacts were limited to the southern and western parts of this forecast region, in the states of Odisha and Chhattisgarh, and some areas beyond that forecast region. Nevertheless, a time series
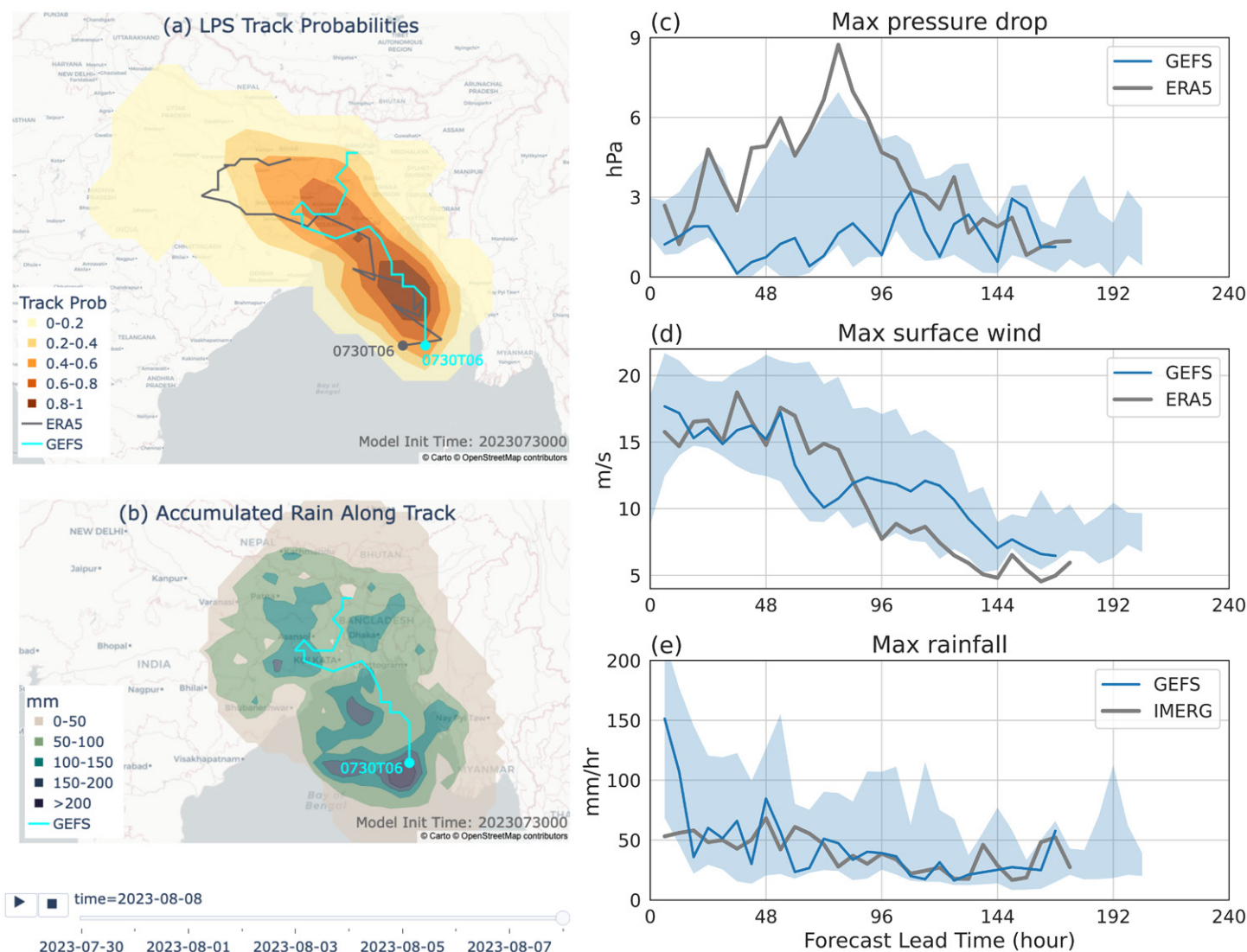
FIG. 3. Snapshot of the operational website for an example LPS. (a) Track probabilities from GEFS forecasts initialized at 0000 UTC 30 Jul 2023, defined as the fraction of ensemble members passing within 1° of each point over the 10 days following initialization. The GEFS control track is shown in cyan and the ERA5 track in gray. Genesis locations are marked by circles with corresponding genesis times. (b) Accumulated rain along the LPS track from the GEFS control, consisting of time-integrated precipitation within 5° of the vortex center. On the website, the time-evolving rain accumulation can be visualized using the slider below the map; here, the static map shows rain accumulated over 10 days since forecast initialization. (right) Forecasts of three intensity metrics: (c) maximum pressure drop between the vortex center and its surroundings (see section 2, optimizing monsoon low pressure system tracking), (d) maximum surface wind speed within 3° of the vortex center, and (e) maximum rainfall within 5° of the vortex center, all from GEFS forecasts initialized 0000 UTC 30 Jul 2023. Blue lines show the control forecast, and blue shading shows the range of the fifth to 95th percentiles of ensemble members (some ensemble members forecast genesis occurring earlier than in the control run or ERA5). Gray lines show observed values from (c)–(d) ERA5 and (e) IMERG.

of the control run's peak rain rates within 5° of the storm-track matched observations well (Fig. 3e; a 5° distance was chosen because it encompasses the majority of the peak rainfall in the composite shown in Fig. 1c); we show in the next section that GEFS forecasts typically underestimate peak LPS rain rates. Overall, this operational system provided several days of advance warning of the location, intensity, and synoptic-scale rain rates of this storm, making that information publicly available in real time through analyses tailored for monsoon LPS.

5. Assessing accuracy to guide forecast use

Having provided a case study of forecasts of one damaging monsoon LPS, we now briefly assess the overall accuracy of the models in forecasting South Asian monsoon LPS in a multiyear period. Specifically, we evaluate the accuracy with which the GEFS and ECMWF

control runs, as well as the deterministic GFS-IITM model, forecast the genesis, position, intensity, and rain rates of South Asian monsoon LPS over the years 2016–22, using ERA5 and IMERG as reference datasets. We choose 2016 as the starting year because the GFS-IITM model has been operational since then, and we assess a longer (15-yr) period for only the GEFS and ECMWF control runs in Figs. S1 and S2. In separate work, Suhas and Boos (2024) show that the GEFS and ECMWF control runs have higher accuracy than nearly all of the perturbed ensemble members from those systems in forecasting the likelihood of genesis. Zhang et al. (2023) and Suhas and Boos (2024) speculated that such greater accuracy of the control runs might be caused by the perturbations added to the ensemble member initial conditions; in any case, this motivates focusing on the control runs here.

a. Genesis. The NWP models predict approximately the correct number of LPS forming in the correct locations each summer but fail to forecast some observed LPSs and predict the formation of other storms that were not observed to form (i.e., the models produce false alarms). Of the 103 LPS events recorded between 2016 and 2022 in ERA5, the GEFS control run successfully predicted ~70% 12 h prior to observed genesis and ~40% 2 days prior to observed genesis (Fig. 4a); this fraction is referred to as the probability of detection (POD), and a successful prediction is as described in the "track comparison methods" section above.

As stated in that section, we use the number of hours prior to observed genesis when assessing POD because POD is defined with respect to an observed event, and model genesis time does not need to exactly match the observed genesis time for a forecast to be deemed a match. The GFS-IITM model has POD values lower than those of the GEFS control run by ~0.1 at most lead times, while the ECMWF control run has values higher by approximately the same amount.

For all models, the POD decreases nearly linearly with increasing time prior to observed genesis, with only ~10% of observed genesis events captured 5 days prior to their observed genesis time. POD values 5 days in advance of observed genesis were likely reduced by our choice to eliminate forecasts where genesis is predicted with lead times > 5 days (see the track comparison methods section), but values 1–3 days before genesis were likely unaffected: Suhas and Boos (2024) obtained a nearly identical 3-day POD when retaining
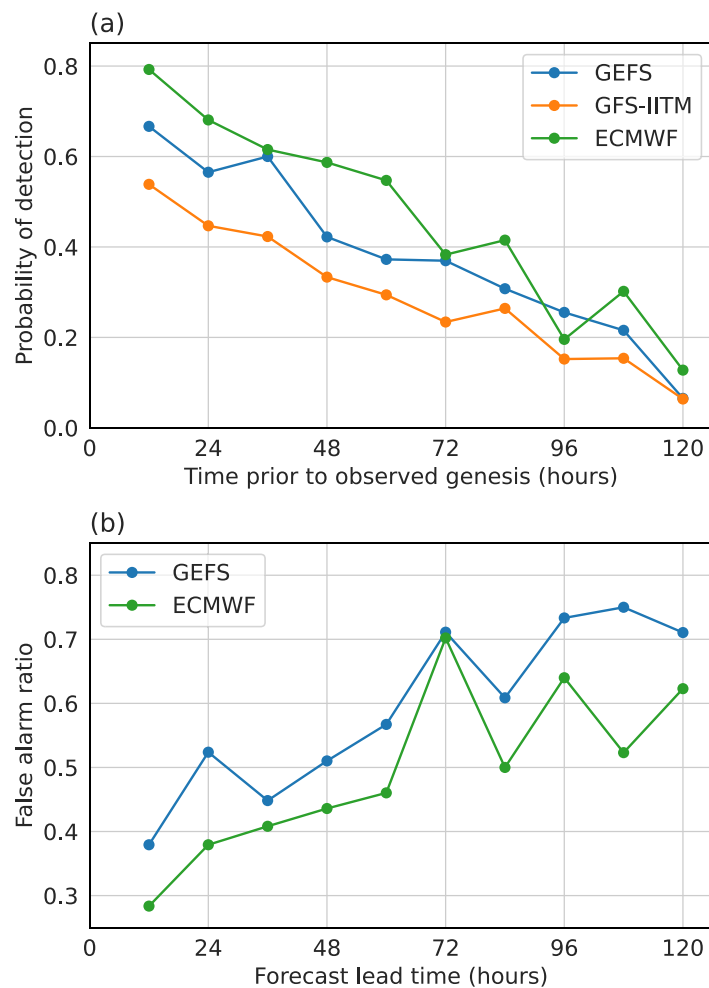

FIG. 4. (a) POD and (b) FAR for LPS genesis forecasts from control runs of the GEFS and ECMWF models and from the deterministic GFS-IITM model, during June–September 2016–22. For GFS-IITM, FAR is not evaluated due to the unavailability of data for all days in the season (see the "data sources and model details" section).

lead times up to 10 days in an analysis of probabilistic predictions for years 2021–22. For an example goal of correctly forecasting at least 50% of observed genesis events, the ECMWF model accomplishes this with ~2.5 days of advance warning, while the GEFS and GFS-IITM models provide ~1.5 and ~0.5 days of warning.

Genesis forecast accuracy also depends on the number of false alarms, defined as LPS forecasts that do not match any observed LPS. The false alarm ratio (FAR), which is the ratio of false alarms to total genesis forecasts made, is ~0.5 for the GEFS control run at a lead time of 2 days (Fig. 4b). The ECMWF model exhibits FAR values lower than those of the GEFS control by ~0.1 at most lead times. In both models, the FAR reaches ~0.6–0.7 for lead times of 3–5 days. Together with the POD values described above, these large false alarm rates at 5 days of lead time (Fig. 4b) further justify focusing on forecasts with shorter (e.g., 1–3 day) lead times.

b. Position and intensity. We now assess the accuracy of LPS location forecasts, which are key to predicting hazard risk for a region. Position error, defined as the total distance between the forecast track location and the ERA5 track location, has a mean value of less than 250 km for all models for lead times up to 4 days (Fig. 5a). This value is only 10%–20% of the outer diameter of a typical LPS (Hurley and Boos 2015), indicating that position errors are typically much smaller than the size of the storms. While the ECMWF control run has a smaller mean position error, this intermodel difference is also small compared to the typical storm diameter. The GFS-IITM model shows mean position errors similar to those of the GEFS control run for lead times up to 3 days; it exhibits larger errors at longer lead times, although the difference is small compared to the standard deviation of these errors.

Although most prior studies of LPS precipitation did not distinguish between monsoon lows and monsoon depressions (e.g., Ajayamohan et al. 2010; Goswami et al. 2006;
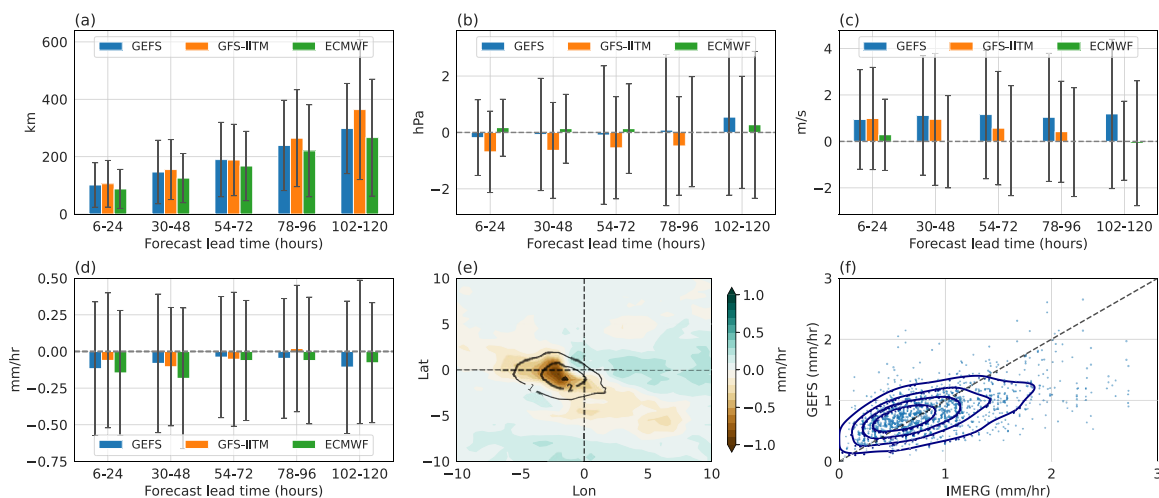

FIG. 5. Model bias as a function of forecast lead time in (a) track position, (b) pressure drop, (c) maximum surface wind speed, and (d) mean precipitation. Biases are obtained by subtracting (a)–(c) ERA5 and (d) IMERG data from the NWP forecasts, with statistics computed over the years 2016–22. Mean values are depicted by colored bars and standard deviations by black error bars. Precipitation biases are spatially averaged within 5° of the LPS center, while pressure drop and maximum winds are as discussed in section 2, optimizing monsoon low pressure system tracking. (e) Storm-centered mean precipitation biases for the GEFS control, averaged over forecast lead times up to 120 h. Observed IMERG precipitation is shown in black contours, with an interval of 1 mm h⁻¹. (f) Comparison of spatially averaged precipitation (within 5° of the LPS center) from IMERG (horizontal axis) with the GEFS control, averaged over forecast lead times up to 120 h (vertical axis). Contours show KDEs with the outer contour enclosing 80% of individual values and the inner contour enclosing 20%. Points indicate individual precipitation values.

You and Ting 2021), recent work showed that depressions produce greater rainfall (Vishnu et al. 2023b) and that more South Asian disasters are associated with depressions than with lows, even though lows occur more frequently (Suhas et al. 2023). Accurately predicting LPS intensity, which is classified by peak surface wind speeds and the pressure drop relative to the background (see the section "optimizing monsoon low pressure system tracking"), is thus important for disaster preparation. Both the GEFS and ECMWF control runs predict the pressure drop well, with near-zero mean bias at most forecast lead times (Fig. 5b). In comparison, the GFS-IITM model underestimates pressure drops by ~0.5 hPa for most lead times, indicating that pressure minima are too weak in that model. Forecasts of surface wind speed maxima are approximately unbiased in the ECMWF control (Fig. 5c), while the GEFS control and GFS-IITM model have positive mean biases less than 1 m s^{-1} in magnitude. Intensity estimates based on wind speed may be less meaningful than those based on pressure drop, because peak wind speeds in LPS may sometimes be elevated due to proximity to the climatological low-level monsoon westerly jet (e.g., Cohen and Boos 2014). Nevertheless, for both metrics, the mean bias is at least several times smaller than the standard deviation, so variation in bias among forecasts will be of greater practical importance for individual cases than average forecast bias.

Accurately predicting LPS rainfall is essential for effective disaster preparedness, as more than 50% of South Asian hydrological disasters in summer are associated with LPS (Suhas et al. 2023). When precipitation is averaged over a 5° circle around the storm center, a region that encompasses the typical location of peak rainfall in the storm's southwest quadrant (e.g., Sanders 1984; Sikka 2006), all three models slightly underestimate precipitation for almost all lead times, with the ECMWF control run exhibiting the largest bias for lead times up to 4 days (Fig. 5d). However, this precipitation bias and intermodel differences are small compared to the standard deviation across forecasts.

The GEFS forecasts capture the observed peak in rainfall southwest of the vortex center (which is shown by black contours in Fig. 5e), but underestimate its magnitude by ~40% and position it farther east than observed (color shading in Fig. 5e shows the model precipitation bias relative to observations, averaged over forecast lead times up to 120 h; the total model precipitation is not shown). The negative precipitation bias in the region of the observed maximum and the positive bias to the east together indicate a weakening and eastward shift of the rainfall peak in the GEFS model relative to observations. Many CMIP6 High Resolution Model Intercomparison Project (HighResMIP) models, which have horizontal resolutions approaching those of the NWP models, also simulated LPS peak precipitation closer to the storm center than in observations (Vishnu et al. 2023a). The NWP models also have difficulty forecasting the most and least intense rain rates. For instance, a scatterplot of horizontal mean precipitation averaged over the first 5 days of lead time reveals that nearly all GEFS control forecasts underestimate rain rates exceeding 1.5 mm h^{-1} in observations and overestimate observed rain rates less than 0.5 mm h^{-1} [Fig. 5f shows individual forecasts as dots with a joint kernel density estimate (KDE) of forecast and observed rain rates]. However, the GEFS control more accurately predicts the most commonly occurring moderate rain rates, as evidenced by the peak in the KDE lying near the 1:1 line. While Figs. 5e and 5f show only GEFS results, the GFS-IITM and ECMWF models exhibit qualitatively similar behavior.

6. Summary and discussion

In this article, we introduced features of an automated operational monsoon LPS forecast system using a case study of a storm that formed over the Bay of Bengal on 30 July 2023 and subsequently produced floods affecting hundreds of thousands of people. The GEFS

successfully predicted the location, peak rain rates, and peak surface wind speeds of this storm several days in advance. Our system makes such custom monsoon LPS diagnostics from GEFS and GFS-IITM forecasts publicly available within $7–12$ h of model initialization. The operational system could, furthermore, be adapted for other regions subject to high societal risk from dynamically weak, heavily precipitating atmospheric vortices that are often excluded from tropical cyclone inventories.

In a 7-yr period of forecasts, the GEFS-based LPS prediction system successfully predicted ~60% of observed genesis events about 1 day in advance, with the ECMWF model successfully predicting ~70% of events and the GFS-IITM model predicting ~45%. The ECMWF model also had fewer false alarms in its forecasts. However, GEFS LPS forecasts have improved over time, with their accuracies approaching those of the ECMWF model in the last 3–5 years (Fig. S1). This helps justify the use of GEFS forecasts in our operational scheme, especially since those are publicly available in real time while ECMWF forecasts are not. LPS genesis forecasts from the GEFS, GFS-IITM, and ECMWF models have generally comparable accuracies to those of tropical cyclone genesis (Halperin et al. 2013, 2016; Zhang et al. 2023). While one might be able to improve the POD score by modifying the quantitative contour-detecting criteria used in the tracking algorithm, such changes might also increase the number of false alarms. Vishnu et al. (2020) tuned the thresholds used here to obtain an optimal combination of hit and false alarm rates between four atmospheric reanalyses and an expert hand-analyzed track dataset and then demonstrated that this tuned algorithm worked well in ERA5 (which was not included in the data used for tuning).

All the models predict the mean position of LPS within 400 km of the observed (i.e., reanalyzed) position for lead times up to 5 days. This is a modest error, less than half the outer radius of a typical LPS (Hurley and Boos 2015) and comparable to that of forecasts of strong tropical cyclones made by operational NWP models in India (Das et al. 2015; Nadimpalli et al. 2020; Routray et al. 2017). The GFS-IITM model underestimated the pressure drop (i.e., the dynamical intensity) of LPS by ~0.5 hPa, resulting in some depressions—which generally produce more rain and hydrological disasters (Suhas et al. 2023)—being incorrectly forecast as lows. We speculate that this underestimation of intensity might be caused by that model's climatological dry bias over India (which might suppress LPS intensification), its initialization procedure, or its subgrid-scale physics. Regardless, this intensity bias is consistent with the finding by Sarkar et al. (2021) that the transition of LPS from lows to depressions occurs too infrequently in the GFS-IITM model.

Perhaps the most important quantity examined here is precipitation, which was forecast in a broadly similar fashion by all three NWP models. The models captured the peak precipitation southwest of the vortex center but underestimated its magnitude (the GEFS underestimate was ~40%). The models also underestimated the highest LPS precipitation rates and overestimated the weakest ones. This behavior provides a clear target for bias correction, although the small number of high-precipitation events may make it difficult to correct the underestimate of intense precipitation. Another promising avenue for improving quantitative LPS precipitation forecasts is a switch to convection-permitting models, such as the regional version of the NCMRWF Regional Unified Model (NCUM-R) run operationally at 4-km horizontal grid spacing for India (Mamgain et al. 2018). However, the fidelity of LPS forecasts in such models still needs to be systematically assessed, since studies have not shown a clear improvement of model representations of LPS at horizontal grid spacing below 25 km (Hunt and Turner 2017; Diaz and Boos 2019b; Hazra and Pattnaik 2021; Vishnu et al. 2023a). Further work is also needed to assess how LPS forecast error is affected by model initialization, model physics, and the climatological dry bias over India in the GFS-based models. Alternatively, LPS properties might be forecast using statistical

or machine learning algorithms instead of dynamical NWP models. The results presented herein provide a reference level of accuracy that such algorithms should achieve to be of practical use.

References

Adames, Á. F., and Y. Ming, 2018: Interactions between water vapor and potential vorticity in synoptic-scale monsoonal disturbances: Moisture vortex instability. *J. Atmos. Sci.*, **75**, 2083–2106, https://doi.org/10.1175/JAS-D-17-0310.1.

Ajayamohan, R. S., W. J. Merryfield, and V. V. Kharin, 2010: Increasing trend of synoptic activity and its relationship with extreme rain events over central India. *J. Climate*, **23**, 1004–1013, https://doi.org/10.1175/2009JCLI2918.1.

Bougeault, P., and Coauthors, 2010: The THORPEX Interactive Grand Global Ensemble. *Bull. Amer. Meteor. Soc.*, **91**, 1059–1072, https://doi.org/10.1175/2010BAMS2853.1.

Cangialosi, J. P., 2021: National Hurricane Center forecast verification report: 2020 Hurricane Season. NOAA/National Hurricane Center Tech. Rep., 77 pp., https://www.nhc.noaa.gov/verification/pdfs/Verification_2020.pdf.

Chakraborty, A., 2016: A synoptic-scale perspective of heavy rainfall over Chennai in November 2015. *Curr. Sci.*, **111**, 201–207, https://doi.org/10.18520/cs/v111/i1/201-207.

Cohen, N. Y., and W. R. Boos, 2014: Has the number of Indian summer monsoon depressions decreased over the last 30 years? *Geophys. Res. Lett.*, **41**, 7846–7853, https://doi.org/10.1002/2014GL061895.

Das, A. K., Y. V. Rama Rao, V. Tallapragada, Z. Zhang, S. K. Roy Bhowmik, and A. Sharma, 2015: Evaluation of the Hurricane Weather Research and Forecasting (HWRF) model for tropical cyclone forecasts over the North Indian Ocean (NIO). *Nat. Hazards*, **75**, 1205–1221, https://doi.org/10.1007/s11069-014-1362-6.

Davidson, N. E., and G. J. Holland, 1987: A diagnostic analysis of two intense monsoon depressions over Australia. *Mon. Wea. Rev.*, **115**, 380–392, https://doi.org/10.1175/1520-0493(1987)115<0380:ADAOTI>2.0.CO;2.

Deoras, A., K. M. R. Hunt, and A. G. Turner, 2021: Comparison of the prediction of Indian monsoon low pressure systems by Subseasonal-to-Seasonal prediction models. *Wea. Forecasting*, **36**, 859–877, https://doi.org/10.1175/WAF-D-20-0081.1.

Diaz, M., and W. R. Boos, 2019a: Barotropic growth of monsoon depressions. *Quart. J. Roy. Meteor. Soc.*, **145**, 824–844, https://doi.org/10.1002/qj.3467.

——, and ——, 2019b: Monsoon depression amplification by moist barotropic instability in a vertically sheared environment. *Quart. J. Roy. Meteor. Soc.*, **145**, 2666–2684, https://doi.org/10.1002/qj.3585.

——, and ——, 2021: Evolution of idealized vortices in monsoon-like shears: Application to monsoon depressions. *J. Atmos. Sci.*, **78**, 1207–1225, https://doi.org/10.1175/JAS-D-20-0286.1.

Directorate General for Civil Protection and Humanitarian Aid Operations, 2023: ECHO Daily Flash of 03 August 2023; European Civil Protection and Humanitarian Aid Operations. ReliefWeb, European Commission's Directorate-General for Civil Protection and Humanitarian Aid Operations, https://reliefweb.int/report/india/india-heavy-rainfall-and-floods-odisha-dg-echo-partners-imd-media-echo-daily-flash-03-august-2023.

Ditchek, S. D., W. R. Boos, S. J. Camargo, and M. K. Tippett, 2016: A genesis index for monsoon disturbances. *J. Climate*, **29**, 5189–5203, https://doi.org/10.1175/JCLI-D-15-0704.1.

Dobhal, D. P., A. K. Gupta, M. Mehta, and D. D. Khandelwal, 2013: Kedarnath disaster: Facts and plausible causes. *Curr. Sci.*, **105**, 171–174.

Dong, W., Y. Ming, and V. Ramaswamy, 2020: Projected changes in South Asian monsoon low pressure systems. *J. Climate*, **33**, 7275–7287, https://doi.org/10.1175/JCLI-D-20-0168.1.

Froude, L. S. R., 2010: TIGGE: Comparison of the prediction of Northern Hemisphere extratropical cyclones by different ensemble prediction systems. *Wea. Forecasting*, **25**, 819–836, https://doi.org/10.1175/2010WAF2222326.1.

Gelaro, R., and Coauthors, 2017: The Modern-Era Retrospective Analysis for Research and Applications, version 2 (MERRA-2). *J. Climate*, **30**, 5419–5454, https://doi.org/10.1175/JCLI-D-16-0758.1.

Goswami, B. N., V. Venugopal, D. Sengupta, M. S. Madhusoodanan, and P. K. Xavier, 2006: Increasing trend of extreme rain events over India in a warming environment. *Science*, **314**, 1442–1445, https://doi.org/10.1126/science.1132027.

Gray, W. M., 1968: Global view of the origin of tropical disturbances and storms. *Mon. Wea. Rev.*, **96**, 669–700, https://doi.org/10.1175/1520-0493(1968)096<0669:GVOTOO>2.0.CO;2.

Guha-Sapir, D., R. Below, and P. Hoyois, 2015: *EM-DAT: International Disaster Database.* Vol. 27. Catholic University of Louvain, 57–58.

Haertel, P., and W. R. Boos, 2017: Global association of the Madden-Julian Oscillation with monsoon lows and depressions. *Geophys. Res. Lett.*, **44**, 8065–8074, https://doi.org/10.1002/2017GL073625.

Halperin, D. J., H. E. Fuelberg, R. E. Hart, J. H. Cossuth, P. Sura, and R. J. Pasch, 2013: An evaluation of tropical cyclone genesis forecasts from global numerical models. *Wea. Forecasting*, **28**, 1423–1445, https://doi.org/10.1175/WAF-D-13-00008.1.

——, ——, ——, and ——, 2016: Verification of tropical cyclone genesis forecasts from global numerical models: Comparisons between the North Atlantic and eastern North Pacific basins. *Wea. Forecasting*, **31**, 947–955, https://doi.org/10.1175/WAF-D-15-0157.1.

Hazra, V., and S. Pattnaik, 2021: Influence of cloud microphysical parameterization on the characteristics of monsoon depressions over the Indian region. *Int. J. Climatol.*, **41**, 6415–6432, https://doi.org/10.1002/joc.7203.

Hersbach, H., and Coauthors, 2020: The ERA5 global reanalysis. *Quart. J. Roy. Meteor. Soc.*, **146**, 1999–2049, https://doi.org/10.1002/qj.3803.

Hodges, K. I., and R. Emerton, 2015: The prediction of Northern Hemisphere tropical cyclone extended life cycles by the ECMWF ensemble and deterministic prediction systems. Part I: Tropical cyclone stage. *Mon. Wea. Rev.*, **143**, 5091–5114, https://doi.org/10.1175/MWR-D-13-00385.1.

Houze, R. A., Jr., K. L. Rasmussen, S. Medina, S. R. Brodzik, and U. Romatschke, 2011: Anomalous atmospheric events leading to the summer 2010 floods in Pakistan. *Bull. Amer. Meteor. Soc.*, **92**, 291–298, https://doi.org/10.1175/2010BAMS3173.1.

——, L. A. McMurdie, K. L. Rasmussen, A. Kumar, and M. M. Chaplin, 2017: Multiscale aspects of the storm producing the June 2013 flooding in Uttarakhand, India. *Mon. Wea. Rev.*, **145**, 4447–4466, https://doi.org/10.1175/MWR-D-17-0004.1.

Huffman, G. J., and Coauthors, 2020: Integrated Multi-satellite Retrievals for the Global Precipitation Measurement (GPM) Mission (IMERG). *Satellite Precipitation Measurement*, V. Levizzani et al., Eds., Advances in Global Change Research, Vol. 1, Springer International Publishing, 343–353, https://doi.org/10.1007/978-3-030-24568-9_19.

Hunt, K. M. R., and A. G. Turner, 2017: The effect of horizontal resolution on Indian monsoon depressions in the Met Office NWP model. *Quart. J. Roy. Meteor. Soc.*, **143**, 1756–1771, https://doi.org/10.1002/qj.3030.

——, and J. K. Fletcher, 2019: The relationship between Indian monsoon rainfall and low-pressure systems. *Climate Dyn.*, **53**, 1859–1871, https://doi.org/10.1007/s00382-019-04744-x.

——, and A. Menon, 2020: The 2018 Kerala floods: A climate change perspective. *Climate Dyn.*, **54**, 2433–2446, https://doi.org/10.1007/s00382-020-05123-7.

Hurley, J. V., and W. R. Boos, 2015: A global climatology of monsoon low-pressure systems. *Quart. J. Roy. Meteor. Soc.*, **141**, 1049–1064, https://doi.org/10.1002/qj.2447.

India Meteorological Department, 2023: Press release, 31st July 2023, 1330 hours IST. S. No. 430, Id. 2457, https://internal.imd.gov.in/pages/press_release_mausam.php.

Jha, A., 2023: Odisha flood: Lakhs affected, villages inundated. *India Today*, 6 August, https://www.indiatoday.in/india/story/odisha-flood-lakhs-affected-villages-inundated-2417183-2023-08-06.

Jones, S. C., 1995: The evolution of vortices in vertical shear. I: Initially barotropic vortices. *Quart. J. Roy. Meteor. Soc.*, **121**, 821–851, https://doi.org/10.1002/qj.49712152406.

Krishnamurti, T. N., M. Kanamitsu, R. Godbole, C.-B. Chang, F. Carr, and J. H. Chow, 1976: Study of a monsoon depression (II), dynamical structure. *J. Meteor. Soc. Japan*, **54**, 208–225, https://doi.org/10.2151/jmsj1965.54.4_208.

Kumar, A., J. Dudhia, R. Rotunno, D. Niyogi, and U. C. Mohanty, 2008: Analysis of the 26 July 2005 heavy rain event over Mumbai, India using the Weather Research and Forecasting (WRF) model. *Quart. J. Roy. Meteor. Soc.*, **134**, 1897–1910, https://doi.org/10.1002/qj.325.

Leung, L. R., and Coauthors, 2022: Exploratory precipitation metrics: Spatiotemporal characteristics, process-oriented, and phenomena-based. *J. Climate*, **35**, 3659–3686, https://doi.org/10.1175/JCLI-D-21-0590.1.

Luo, H., Á. F. Adames Corraliza, and R. B. Rood, 2023: Barotropic and moisture–vortex growth of monsoon low pressure systems. *J. Atmos. Sci.*, **80**, 2823–2836, https://doi.org/10.1175/JAS-D-22-0252.1.

Mahanti, T. K., 2022: Religious tourism turns economic multiplier across globe. *Business Economics Magazine*, 1 November 2022, https://businesseconomics.in/religious-tourism-turns-economic-multiplier-across-globe.

Mamgain, A., E. N. Rajagopal, A. K. Mitra, and S. Webster, 2018: Short-range prediction of monsoon precipitation by NCMRWF regional unified model with explicit convection. *Pure Appl. Geophys.*, **175**, 1197–1218, https://doi.org/10.1007/s00024-017-1754-0.

Ministry of Home Affairs, 2023a: Situation report regarding flood and heavy rainfall in the country (03/08/2023, 1800 hrs). ReliefWeb, United Nations Office for the Coordination of Humanitarian Affairs, 6 pp., https://reliefweb.int/report/india/ministry-home-affairs-disaster-management-division-national-emergency-response-centre-situation-report-regarding-flood-heavy-rainfall-country-03082023-1800-hrs.

——, 2023b: Situation report regarding flood and heavy rainfall in the country (04/08/2023, 1800 hrs). ReliefWeb, United Nations Office for the Coordination of Humanitarian Affairs, 6 pp., https://reliefweb.int/report/india/ministry-home-affairs-disaster-management-division-national-emergency-response-centre-situation-report-regarding-flood-heavy-rainfall-country-04082023-1800-hrs.

Mooley, D. A., and J. Shukla, 1987: Characteristics of the westward-moving summer monsoon low pressure systems over the Indian region and their relationship with the monsoon rainfall. University of Maryland Center for Ocean-Land-Atmosphere Interactions Rep., 47 pp.

Mukhopadhyay, P., and Coauthors, 2019: Performance of a very high-resolution global forecast system model (GFS T1534) at 12.5 km over the Indian region during the 2016–2017 monsoon seasons. *J. Earth Syst. Sci.*, **128**, 155, https://doi.org/10.1007/s12040-019-1186-6.

——, and Coauthors, 2021: Unraveling the mechanism of extreme (more than 30 sigma) precipitation during August 2018 and 2019 over Kerala, India. *Wea. Forecasting*, **36**, 1253–1273, https://doi.org/10.1175/WAF-D-20-0162.1.

Nadimpalli, R., K. K. Osuri, U. C. Mohanty, A. K. Das, A. Kumar, S. Sil, and D. Niyogi, 2020: Forecasting tropical cyclones in the Bay of Bengal using quasi-operational WRF and HWRF modeling systems: An assessment study. *Meteor. Atmos. Phys.*, **132** (1), 1–17, https://doi.org/10.1007/s00703-019-00669-6.

Nikumbh, A. C., A. Chakraborty, G. S. Bhat, and D. M. W. Frierson, 2020: Large-scale extreme rainfall-producing synoptic systems of the Indian summer monsoon. *Geophys. Res. Lett.*, **47**, e2020GL088403, https://doi.org/10.1029/2020GL088403.

Park, Y.-Y., R. Buizza, and M. Leutbecher, 2008: TIGGE: Preliminary results on comparing and combining ensembles. *Quart. J. Roy. Meteor. Soc.*, **134**, 2029–2050, https://doi.org/10.1002/qj.334.

Prasad, V. S., C. J. Johny, and J. S. Sodhi, 2016: Impact of 3D Var GSI-ENKF hybrid data assimilation system. *J. Earth Syst. Sci.*, **125**, 1509–1521, https://doi.org/10.1007/s12040-016-0761-3.

Press Trust of India, 2023: Odisha flood: Lakhs affected, villages inundated. *Deccan Herald*, 7 August 2023, https://www.deccanherald.com/india/odisha/od-flood-2-2637218.

Rao, K. V., and S. Rajamani, 1970: Diagnostic study of a monsoon depression by geostrophic baroclinic model. *Mausam*, **21**, 187–194, https://doi.org/10.54302/mausam.v21i2.5366.

Routray, A., V. Singh, J. P. George, S. Mohandas, and E. N. Rajagopal, 2017: Simulation of tropical cyclones over Bay of Bengal with NCMRWF regional unified model. *Pure Appl. Geophys.*, **174**, 1101–1119, https://doi.org/10.1007/s00024-016-1447-0.

Sampson, C. R., and A. J. Schrader, 2000: The Automated Tropical Cyclone Forecasting System (version 3.2). *Bull. Amer. Meteor. Soc.*, **81**, 1231–1240, https://doi.org/10.1175/1520-0477(2000)081<1231:TATCFS>2.3.CO;2.

Sanders, F., 1984: Quasi-geostrophic diagnosis of the monsoon depression of 5–8 July 1979. *J. Atmos. Sci.*, **41**, 538–552, https://doi.org/10.1175/1520-0469(1984)041<0538:QGDOTM>2.0.CO;2.

Sarkar, S., P. Mukhopadhyay, S. Dutta, R. Phani Murali Krishna, R. D. Kanase, V. S. Prasad, and M. S. Deshpande, 2021: GFS model fidelity in capturing the transition of low-pressure area to monsoon depression. *Quart. J. Roy. Meteor. Soc.*, **147**, 2625–2637, https://doi.org/10.1002/qj.4024.

Sati, S. P., and V. K Gahalaut, 2013: The fury of the floods in the north-west Himalayan region: The Kedarnath tragedy. *Geomatics Nat. Hazards Risk*, **4**, 193–201, https://doi.org/10.1080/19475705.2013.827135.

Sati, V. P., 2020: The trends of tourism and tourists/pilgrims' inflow. *Sustainable Tourism Development in the Himalaya: Constraints and Prospects*, Springer, 53–66, https://doi.org/10.1007/978-3-030-58854-0_5.

Sikka, D. R., 1977: Some aspects of the life history, structure and movement of monsoon depressions. *Pure Appl. Geophys.*, **115**, 1501–1529, https://doi.org/10.1007/BF00874421.

——, 2006: A study on the monsoon low pressure systems over the Indian region and their relationship with drought and excess monsoon seasonal rainfall. Center for Ocean-Land-Atmosphere Studies Tech. Rep. 217, 61 pp.

Suhas, D. L., and W. R. Boos, 2023: Monsoon depression amplification by horizontal shear and humidity gradients: A shallow water perspective. *J. Atmos. Sci.*, **80**, 633–647, https://doi.org/10.1175/JAS-D-22-0146.1.

——, and ——, 2024: Evaluating ensemble predictions of South Asian monsoon low pressure system genesis. *Wea. Forecasting*, **39**, 1377–1386, https://doi.org/10.1175/WAF-D-24-0044.1.

——, N. Ramesh, R. M. Kripa, and W. R. Boos, 2023: Influence of monsoon low pressure systems on South Asian disasters and implications for disaster prediction. *npj Climate Atmos. Sci.*, **6**, 48, https://doi.org/10.1038/s41612-023-00376-5.

Swinbank, R., and Coauthors, 2016: The TIGGE project and its achievements. *Bull. Amer. Meteor. Soc.*, **97**, 49–67, https://doi.org/10.1175/BAMS-D-13-00191.1.

Ullrich, P. A., C. M. Zarzycki, E. E. McClenny, M. C. Pinheiro, A. M. Stansfield, and K. A. Reed, 2021: TempestExtremes v2.1: A community framework for feature detection, tracking, and analysis in large datasets. *Geosci. Model Dev.*, **14**, 5023–5048, https://doi.org/10.5194/gmd-14-5023-2021.

Vishnu, S., W. R. Boos, P. A. Ullrich, and T. A. O'Brien, 2020: Assessing historical variability of South Asian monsoon lows and depressions with an optimized tracking algorithm. *J. Geophys. Res. Atmos.*, **125**, e2020JD032977, https://doi.org/10.1029/2020JD032977.

——, ——, and W. D. Collins, 2023a: Historical and future trends in South Asian monsoon low pressure systems in a high-resolution model ensemble. *npj Climate Atmos. Sci.*, **6**, 182, https://doi.org/10.1038/s41612-023-00502-3.

——, M. D. Risser, T. A. O'Brien, P. A. Ullrich, and W. R. Boos, 2023b: Observed increase in the peak rain rates of monsoon depressions. *npj Climate Atmos. Sci.*, **6**, 111, https://doi.org/10.1038/s41612-023-00436-w.

Walch, C., 2019: Adaptive governance in the developing world: Disaster risk reduction in the State of Odisha, India. *Climate Dev.*, **11**, 238–252, https://doi.org/10.1080/17565529.2018.1442794.

You, Y., and M. Ting, 2021: Observed trends in the South Asian monsoon low-pressure systems and rainfall extremes since the late 1970s. *Geophys. Res. Lett.*, **48**, e2021GL092378, https://doi.org/10.1029/2021GL092378.

Yu, H., P. Chen, Q. Li, and B. Tang, 2013: Current capability of operational numerical models in predicting tropical cyclone intensity in the western North Pacific. *Wea. Forecasting*, **28**, 353–367, https://doi.org/10.1175/WAF-D-11-00100.1.

Zhang, X., J. Fang, and Z. Yu, 2023: The forecast skill of tropical cyclone genesis in two global ensembles. *Wea. Forecasting*, **38**, 83–97, https://doi.org/10.1175/WAF-D-22-0145.1.

Zhou, X., and Coauthors, 2022: The development of the NCEP Global Ensemble Forecast System version 12. *Wea. Forecasting*, **37**, 1069–1084, https://doi.org/10.1175/WAF-D-21-0112.1.